Communication

Propeller-Shaped Aluminum Complexes with an Azaperylene Core in the Ligands

Masahiro Tsukao [1], Yoshifumi Hashikawa [1] , Nana Toyama [2], Masahiro Muraoka [3] , Michihisa Murata [3,4,]* , Takahiro Sasamori [5], Atsushi Wakamiya [1] and Yasujiro Murata [1,]*

[1] Institute for Chemical Research, Kyoto University, Uji, Kyoto 611-0011, Japan
[2] Graduate School of Engineering, Osaka Institute of Technology, 5-16-1 Omiya, Asahi-ku, Osaka 535-8585, Japan
[3] Department of Applied Chemistry, Faculty of Engineering, Osaka Institute of Technology, 5-16-1 Omiya, Asahi-ku, Osaka 535-8585, Japan
[4] JST-PRESTO, 4-1-8 Honcho, Kawaguchi, Saitama 332-0012, Japan
[5] Graduate School of Natural Sciences, Nagoya City University, Yamanohata 1, Mizuho-cho, Mizuho-ku, Nagoya, Aichi 467-8501, Japan
[*] Correspondence: michihisa.murata@oit.ac.jp (M.M.); yasujiro@scl.kyoto-u.ac.jp (Y.M.)

check for updates

Abstract: Tris(8-hydroxyquinoline) aluminum(III) (Alq_3) and its derivatives, characterized by a propeller-shaped three-dimensionally π-conjugated structure, have been intensively studied in the few past decades on account of their potential utility in optoelectronic applications. Reported herein are the synthesis and properties of π-extended Alq_3 complexes that contain an azaperylene core in each ligand. Intramolecular palladium-catalyzed direct C–H arylations or base-promoted arylations were employed to prepare these large Alq_3 analogues. A single-crystal X-ray diffraction analysis of one of the obtained Al complexes revealed a unique three-dimensional packing structure within the crystal, i.e., a honeycomb packing along the *ab*-plane and columnar π-stacks along the *c*-axis. An Alq_3 analogue with azaperylene-dicarboximide ligands exhibited deep blue color in solution with an intense absorption band that extended to 780 nm ($\lambda_{\max}$ = 634 nm; ε = 58,000 M^{-1} cm^{-1}).

Keywords: Alq_3; 8-hydoxyquinoline; annulation; direct C–H arylation; perylene; PAH

1. Introduction

Three-dimensional (3D) π-conjugated systems have received increasing attention as charge-transporting materials for thin-film devices [1–12]. While two-dimensional (2D) planar π-systems often exhibit an anisotropic charge transport depending on their orientation in the film (face-on or edge-on relative to the substrate), 3D nonplanar π-systems may potentially exhibit isotropic charge-transport behavior. Recently, Sisto and co-workers reported that 3D nanostructures, in which three graphene nanoribbons are covalently attached to a triptycene core, can be used as electron-extracting layers in perovskite solar cells [12]. Zhang and co-workers reported a 3D nanostructure comprised of three perylene-dicarboximide units covalently attached to a [3,3,3]propellane core that exhibits an isotropic charge transport despite the weak intermolecular contact between the π-conjugated moieties [5]. Substantial efforts have also been devoted to developing non-fullerene-type acceptor materials for organic photovoltaics (OPVs) based on twisted 3D π-systems given their positive influence on the morphology of films mixed with donor polymers [6–11].

Among the 3D π-systems, tris(8-hydroxyquinoline) aluminum(III) (Alq_3), which exhibits a propeller-shaped structure, is often encountered in OLEDs as a stable, light-emitting, and electron-transporting material [13,14]. The aluminum(III) ion plays a critical role in the

well-controlled structure of the 3D π-system, in which three 8-hydroxyquinolinato ligands are assembled in a propeller shape that allows for two stereoisomers: Meridional (*mer*) and facial (*fac*) isomers with C_1- and C_3-symmetric point groups, respectively. In the past few decades, the properties, structures, and ligand-exchange dynamics of Alq_3 have been extensively studied, both in solutions and in the solid state [15–17]. The properties of Alq_3 can be tuned via the introduction of functional group(s) in the 8-hydroxyquinolinato ligands of Alq_3 [18–23]. Even though 3D π-systems can be readily obtained by using metal-coordination, the π-extension of the ligands in Alq_3 derivatives by annulation has remained largely unexplored. We envisioned that 3D π-systems with enhanced intermolecular π–π interactions could potentially be obtained by introducing a naphthalene-fused structure to the ligands of Alq_3 (Figure 1). Herein, we report the synthesis and properties of π-extended Alq_3 derivatives that contain azaperylene or azaperylene-dicarboximide units by intramolecular palladium-catalyzed direct C–H arylation or base-promoted arylation. The unique packing structure of the naphthalene-fused Alq_3 with an intense visible absorption was unambiguously revealed by single-crystal X-ray diffraction analysis.
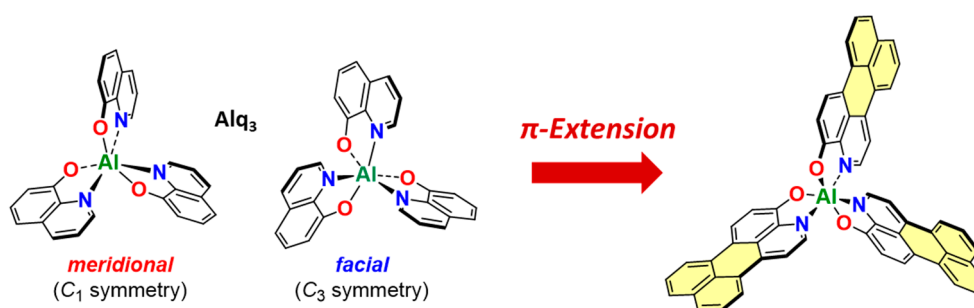

Figure 1. Chemical structures of Alq_3 stereoisomers and of a π-extended Alq_3 that contains an azaperylene unit in each ligand.

2. Results and Discussion

The synthesis of the naphthalene-fused ligands was accomplished using precursor **1**, which contains a methoxy group in order to increase the reactivity toward the intramolecular Pd-catalyzed direct C–H arylations (Scheme 1) [24–30]. Precursor **1** contains two possible reaction sites for direct arylation at the quinoline core (indicated with arrows in Scheme 1). During the optimization of the reaction conditions, we found that adding pivalic acid (PivOH) under the decreased reaction temperature allowed us to control the cyclization mode (Table 1). The microwave-assisted heating of an *N*-methylpyrrolidone (NMP) solution containing **1**, $Pd(OAc)_2$, $PCy_3·HBF_4$ (ligand), and K_2CO_3 (base) to 170 °C afforded π-extended **2** (48%) and its regioisomer **3** (12%) due to the formation of hexagonal and pentagonal rings, respectively (Table 1, entry 1). When PivOH was used as an additive, the yield of **3** improved (21%), while the yield of **2** remained virtually unchanged (47%) (Table 1, entry 2). Upon decreasing the reaction temperature, the formation of **2** was not observed, and **3** (20%) was generated exclusively (Table 1, entry 3). PivOH has been reported to act as a proton shuttle in a concerted metalation–deprotonation (CMD) pathway of Pd-catalyzed direct arylations [25]. Thus, the obtained results indicate that the CMD pathway favors the cyclization that furnishes **3**, while the formation of **2** proceeds via a different pathway, e.g., a Heck-type coupling reaction. The structure of **2** was unambiguously determined by a single-crystal X-ray diffraction analysis (cf. Supplementary Materials).

Control over the selectivity in Pd-catalyzed direct arylation reactions has recently been reported by Würthner and co-workers, who demonstrated that in the synthesis of electron-deficient polycyclic aromatic dicarboximides, intramolecular cyclization modes under the formation of hexagonal and pentagonal rings can be addressed by the judicious choice of the auxiliary base such as Cs_2CO_3 or diazabicycloundecene (DBU) [31]. In our case, the annulation mode was controlled by the use of a catalytic amount of PivOH under a decreased reaction temperature. To gain better insight

into the mechanisms that underpin these catalytic systems, we conducted DFT calculations at the M06-2x/6-31G** (C, H, N, O, P)/SDD (Pd) level of theory [32]. In the absence of PivOH, the calculated barrier for the Heck-type pathway via transition-state (TS) **I** (Figure 2) to give **2** was lower than the barrier for the formation of **3**, i.e., $\Delta G^{\ddagger} = +34.0$ and $+48.7$ kcal/mol for the formation of **2** and **3**, respectively (cf. Supplementary Materials) [33–35]. On the other hand, in the presence of PivOH, the calculated barrier for the CMD pathway via TS **II** (Figure 2) to give **2** was higher than the barrier for the formation of **3**, i.e., $\Delta G^{\ddagger} = +46.9$ and $+33.5$ kcal/mol (L = NMP) [30] for the formation of **2** and **3**, respectively (cf. Supplementary Materials). The selectivity of the annulation mode upon using PivOH can probably be ascribed to the steric constraints in the transition states for both the Heck-type and the CMD pathways. The obtained products were subsequently deprotected with sodium thiomethoxide to furnish the naphthalene-fused ligand **L1** and its regioisomer **L2** [36].
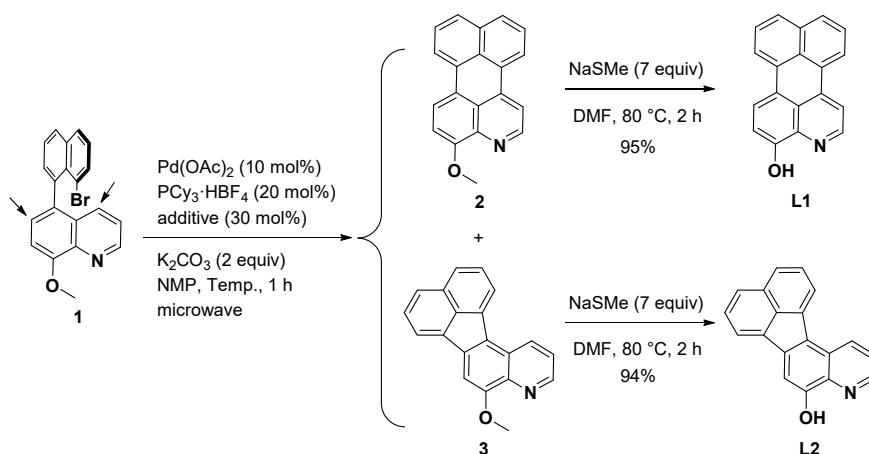

Scheme 1. Synthetic routes to naphthalene-fused quinolinol ligands via an intramolecular palladium-catalyzed direct arylation followed by deprotection; PCy$_3$: Tricyclohexylphosphine; NMP: *N*-methylpyrrolidone.

Table 1. Optimization of the reaction conditions for the synthesis of **2** and **3**.

Entry	Additive	Temp. (°C)	Yield (%) [1]	
			2	**3**
1	–	170	48	12
2	PivOH	170	47	21
3	PivOH	120	0	20

[1] Isolated yield; PivOH: Pivalic acid.
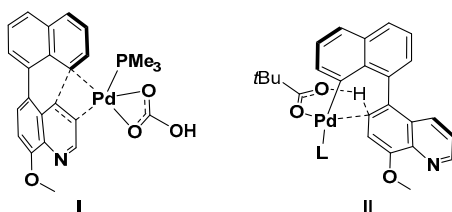
Figure 2. Transition-states **I** and **II** for the formation of **2** and **3** via Heck-type and concerted metalation–deprotonation (CMD) pathways, respectively.

Owing to the presence of a strong electron-withdrawing group, the intramolecular cyclization of precursor **4** could be carried out by base-promoted direct arylation [37,38]. Product **5** was subsequently deprotected to provide ligand **L3** with an azaperylene-dicarboximide unit (Scheme 2), and its structure was unequivocally confirmed by a single-crystal X-ray diffraction analysis.
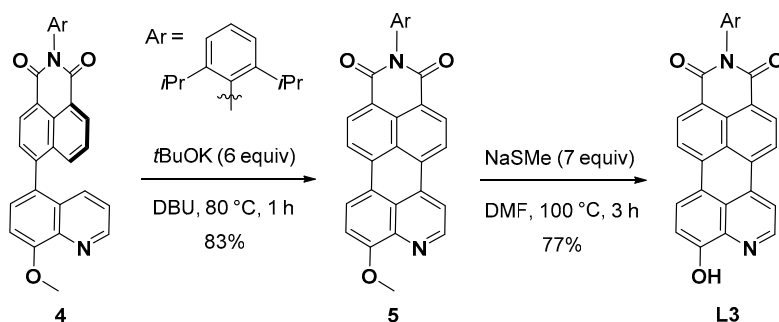
Scheme 2. Base-promoted intramolecular cyclization of **4** and subsequent deprotection of **5** to generate **L3**.

The synthesis of the propeller-shaped aluminum complex Al(**L1**)$_3$ was accomplished by treating the **L1** ligand with aluminum trichloride (Scheme 3). Al(**L1**)$_3$ was obtained as a dark purple solid, which was hardly soluble in common organic solvents, except for 1,1,2,2-tetrachloroethane (TCE), benzonitrile, and 1,2-dichlorobenzene (ODCB). While Al(**L2**)$_3$ exhibited solubility similar to that of Al(**L1**)$_3$, the dark blue solid of Al(**L3**)$_3$, which contained three bulky dicarboximide moieties (Scheme 3), showed an improved solubility in organic solvents such as chloroform and dichloromethane. The APCI mass spectrum of Al(**L3**)$_3$ clearly exhibited the molecular ion peak [M]$^-$. The ^{1}H NMR spectrum of Al(**L3**)$_3$ in CDCl$_3$ indicated that the complex adopted C_1 symmetry, i.e., the meridional form was present in CDCl$_3$ judging from the aromatic proton signals arising from three nonequivalent azaperylene moieties. DFT calculations at the B3LYP/6-31G* level of theory for Al(**L3′**)$_3$ (Ar = methyl for simplification) suggest that the meridional isomer was more stable than the facial isomer by $\Delta E = 4.8$ kcal/mol, and it was almost identical to the stabilization of the meridional form of Alq$_3$ ($\Delta E = 5.0$ kcal/mol). Accordingly, our calculations agree well with the experimental results.
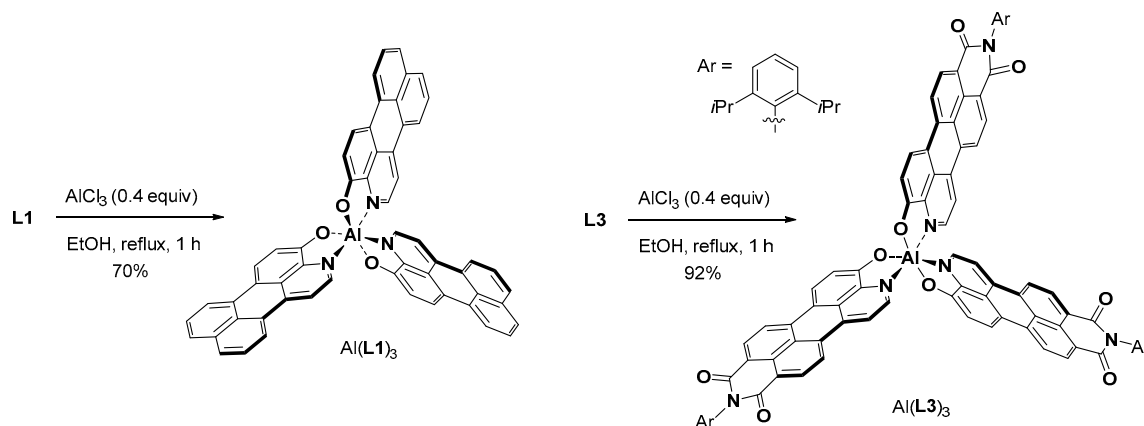

Scheme 3. Formation of the propeller-shaped complexes Al(**L1**)$_3$ and Al(**L3**)$_3$.

A single crystal of Al(**L1**)$_3$ was obtained by the slow diffusion of acetonitrile into an ODCB solution of Al(**L1**)$_3$. The structure of Al(**L1**)$_3$ was unambiguously determined by a single-crystal X-ray diffraction analysis, which revealed that the crystal contained acetonitrile and the meridional isomer of Al(**L1**)$_3$. The packing structure of *mer*-Al(**L1**)$_3$ within the crystal was characterized by a two-dimensional honeycomb-type arrangement of the two enantiomers, namely the Λ and Δ forms [39,40], in the *ab*-plane (Figure 3a). Each enantiomer of *mer*-Al(**L1**)$_3$ formed one-dimensional π-stacks with a rotation of the three ligands along the *c*-axis (Figure 3b). The intermolecular distances of the π-stacks (3.3–3.5 Å) within the crystal of *mer*-Al(**L1**)$_3$ were shorter than those reported for *mer*-Alq$_3$ (3.5–3.9 Å) [41], reflecting the enhanced π–π interactions between the π-extended ligands.
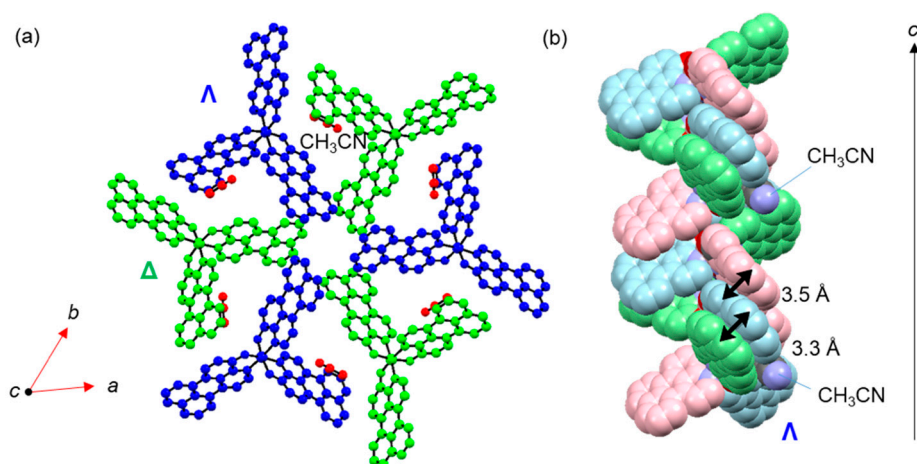
Figure 3. X-ray crystal structure of Al(**L1**)$_3$. (**a**) Two-dimensional honeycomb-type packing in the *ab*-plane and (**b**) one-dimensional π-stacks along the *c*-axis within the crystal. Thermal ellipsoids are shown at 50% probability.

To examine the electronic properties, the absorption spectra of the ligands as well as their aluminum complexes were recorded (Figure 4). The obtained results indicate that the absorption bands of the aluminum complexes were notably red-shifted with respect to those of the ligands. For example, the intense absorption band of Al(**L3**)$_3$ (λ_{max} = 634 nm; log ε = 4.76), which was blue in solution, was bathochromically shifted by 100 nm with respect to that of **L3** (λ_{max} = 534 nm; log ε = 4.31). The characteristics of Al(**L1**)$_3$ (λ_{max} = 556 nm; logε = 4.54) and Al(**L3**)$_3$ (λ_{max} = 634 nm; log ε = 4.76) were the broad absorption bands in the visible range tailing up to 640 and 780 nm, respectively, with a remarkably high molar absorptivity compared to that of Alq$_3$ (λ_{max} = 388 nm; log ε = 3.83) and [6,6]-phenyl-C$_{60}$-butyric acid methyl ester (PCBM, λ_{max} = 430 nm; log ε = 3.2), which is used as the acceptor material in OPVs [42,43]. DFT calculations for Al(**L1**)$_3$ and Al(**L3**)$_3$ at the B3LYP/6-31G* level of theory suggest that the π-conjugation did not include multiple ligands through the aluminum center, but that it was rather localized on each ligand, which reflected the C_1 symmetry of the meridional form (Figure 5). While the longest wavelength absorptions of Al(**L1**)$_3$ and Al(**L3**)$_3$ could be assigned to the two overlapping transitions with dominant contributions of localized π–π* transitions in each ligand, there were also minor contributions with the intramolecular charge-transfer (ICT) character, which corresponded to the transitions across the different ligands (Table 2). The cyclic voltammogram of Al(**L3**)$_3$ exhibited a reversible reduction wave ($E_{1/2}$ = −1.29 V vs Fc/Fc$^+$) that was almost identical to that of **L3** ($E_{1/2}$ = −1.31 V), indicating a high electron affinity for Al(**L3**)$_3$ due to the dicarboximide groups with strongly electron-withdrawing properties.
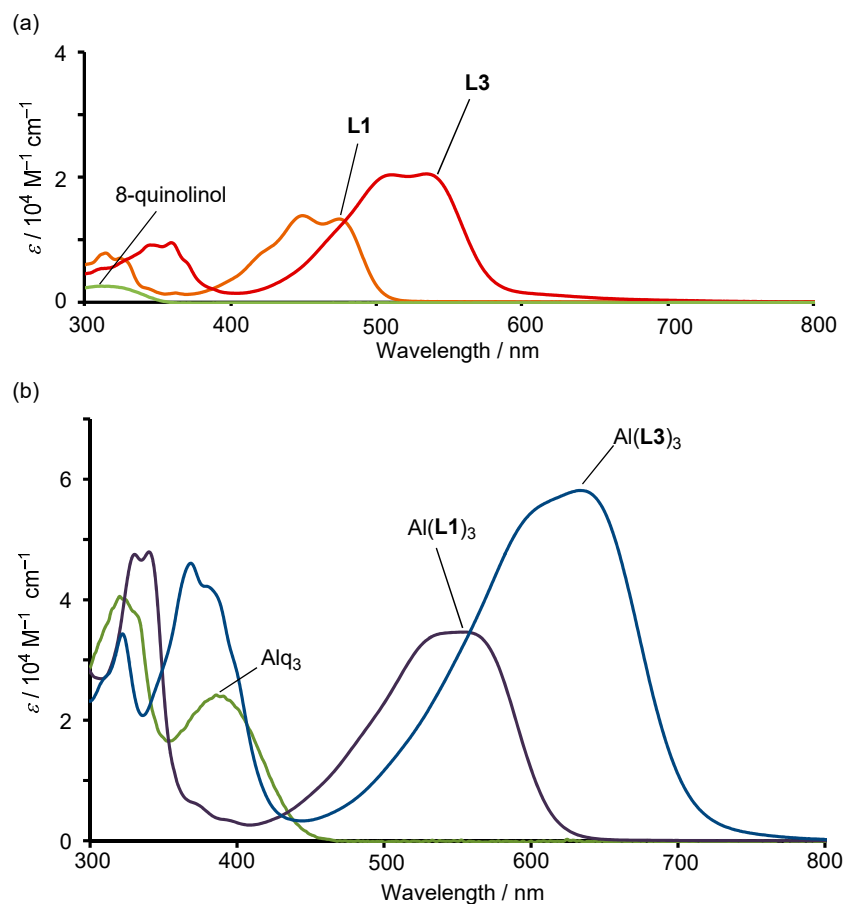
Figure 4. UV–Vis absorption spectra of (**a**) the ligands 8-quinolinol, **L1**, and **L3**, as well as (**b**) the aluminum complexes Alq_3, $Al(\textbf{L1})_3$, and $Al(\textbf{L3})_3$. All spectra were measured in CH_2Cl_2 except for that of $Al(\textbf{L1})_3$, which was measured in 1,1,2,2-tetrachloroethane (TCE) due to the low solubility of $Al(\textbf{L1})_3$ in other common organic solvents.
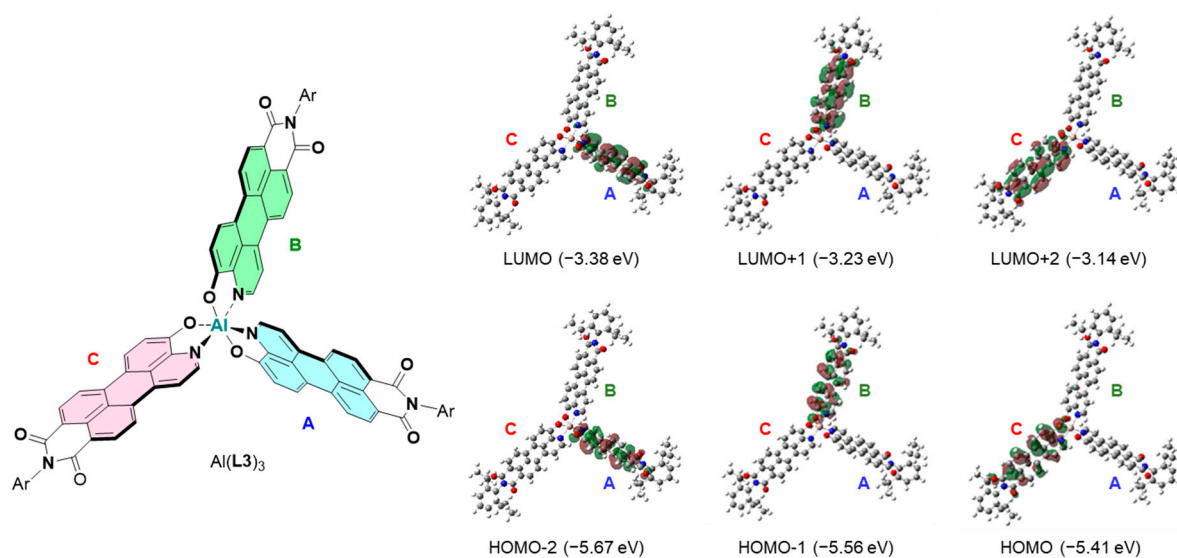
Figure 5. Selected frontier orbitals of the meridional isomer of $Al(\textbf{L3})_3$ for the optimized ground-state structure calculated at the B3LYP/6-31G* level of theory.

Table 2. Main electronic transitions for *mer*-Al(**L3**)$_3$, calculated at the TD-CAM-B3LYP/6-31G*// B3LYP/6-31G* level of theory.

λ$_{calculated}$ (nm)	Oscillator Strength	Contributing MOs (%) [1]	Character
546	0.916	HOMO → LUMO+2 (58) HOMO–2 → LUMO (19) HOMO → LUMO+1 (10)	π→π* π→π* ICT
536	0.861	HOMO–2 → LUMO (45) HOMO–1 → LUMO+1 (36) HOMO → LUMO+1 (5)	π→π* π→π* ICT

[1] The corresponding orbitals are shown in Figure 5.

3. Materials and methods

The ^{1}H and ^{13}C NMR measurements were carried out with a JEOL JNM-ECA 500 instrument (JEOL Ltd., Tokyo, Japan). The NMR chemical shifts were reported in ppm with reference to residual protons and carbons of CDCl$_3$ (δ 7.26 ppm in ^{1}H NMR and δ 77.0 ppm in ^{13}C NMR), CD$_2$Cl$_2$ (δ 5.33 ppm in ^{1}H NMR and δ 54.2 ppm in ^{13}C NMR), and tetrachloroethane-d_2 (δ 6.00 ppm in ^{1}H NMR). UV–Vis absorption spectra were measured with a Shimadzu UV-3150 spectrometer (Shimadzu Corp., Kyoto, Japan). APCI and ESI mass spectra were measured on Bruker micrOTOF-Q II spectrometer (Bruker Japan K.K., Kanagawa, Japan). The microwave reaction was performed using an Anton Paar Monowave 300 (Anton Paar Japan K.K., Tokyo, Japan). Cyclic voltammetry (CV) was performed on a BAS ALS620A electrochemical analyzer (BAS Inc., Tokyo, Japan). The CV cell consisted of a glassy carbon electrode, a Pt wire counter electrode, and an Ag/AgNO$_3$ reference electrode. The measurements were carried out under an argon atmosphere using a CH$_2$Cl$_2$ solution of a sample with a concentration of 1 mM and 0.1 M tetrabutylammonium hexafluorophosphate (nBu$_4$N$^+$PF$_6{}^-$) as a supporting electrolyte. The redox potentials were calibrated with ferrocene as an internal standard. *t*BuOH, diazabicycloundecene (DBU), 3-aminopentane were purchased from Tokyo Chemical Industry Co., Ltd. (Tokyo, Japan). 4-Bromo-1,8-naphthalic anhydride, 2,6-diisopropylaniline, propionic acid, K$_3$PO$_4$, PCy$_3$·HBF$_4$, DMF, PivOH, Pd(OAc)$_2$, *N*-methylpyrrolidone (NMP), AlCl$_3$, K$_2$CO$_3$, aniline were purchased from FUJIFILM Wako Pure Chemical Corporation (Osaka, Japan). Sodium thiomethoxide was purchased from Sigma-Aldrich Co. LLC. (Tokyo, Japan). *N*-Hexylamine was purchased from Nacalai Tesque, Inc. (Kyoto, Japan). Compound **1A**[1] and **4A**[2] were prepared according to the literature.

All calculations were conducted with Gaussian 09 packages (Gaussian, Inc., Wallingford, CT, USA). The structures were fully optimized with the B3LYP functional and basis set of 6-31G* without any symmetry assumptions. For the computational analyses of the mechanism of the Pd-catalyzed direct arylation reactions, calculations were performed by the M06-2X with a combined basis set, i.e., SDD for Pd and 6-31G** for the rest. Optical transitions with oscillator strength were calculated at the TD-CAM-B3LYP/6-31G* level of theory.

3.1. Synthesis of Compound **1**

Compound **1A** (513 mg, 1.80 mmol), *o*-dibromonaphthalene (1.03 g, 3.60 mmol), Pd$_2$(dba)$_3$·CHCl$_3$ (56.0 mg, 0.0540 mmol), PPh$_3$ (56.7 mg, 0.216 mmol) and K$_3$PO$_4$ (1.15 g, 5.40 mmol) were suspended in a mixed solvent of DMF/H$_2$O (10:1, 33 mL) and stirred for 5 h at 80 °C under an argon atmosphere. The reaction mixture was cooled to room temperature and diluted with EtOAc. The organic layer was washed three times with water, and the aqueous layer was extracted three times with EtOAc. The organic layer was combined, dried over Na$_2$SO$_4$, and evaporated under a reduced pressure. The crude product was purified by column chromatography on silica gel (CH$_2$Cl$_2$/AcOEt, 10:1) to give **1** (495 mg, 1.36 mmol) in a 75% yield as colorless solids. Data for **1**: ^{1}H NMR (500 MHz, CDCl$_3$): δ 8.97 (dd, *J* = 2.0, 0.8 Hz, 1H), 8.04 (dd, *J* = 4.3, 1.0 Hz, 1H), 8.00 (dd, *J* = 4.0, 0.5 Hz, 1H), 7.77 (dd, *J* = 3.4, 1.0 Hz, 1H), 7.62 (m, 2H), 7.54 (dd, *J* = 3.8, 1.0 Hz, 1H), 7.43 (d, *J* = 4.0 Hz, 1H), 7.36 (t, *J* = 3.8 Hz,

1H), 7.25 (dd, *J* = 4.3, 2.0 Hz, 1H), 7.11 (d, *J* = 3.8 Hz, 1H), and 4.17 (s, 3H); ^{13}C NMR (126 MHz, CDCl$_3$): δ 155.01, 148.80, 139.60, 136.52, 135.84, 134.47, 133.80, 132.20, 132.11, 130.61, 130.21, 129.59, 129.07, 127.90, 126.17, 125.44, 121.46, 119.67, 106.74 and, 55.94; HRMS (+APCI): [M + H]$^+$ calculated for C$_{20}$H$_{15}$BrNO 364.0332, found 364.0322.

3.2. Synthesis of Compounds 2 and 3

Compound **1** (726 mg, 1.99 mmol), Pd(OAc)$_2$ (45.5 mg, 0.203 mmol), PCy$_3$·HBF$_4$ (148 mg, 0.0401 mmol) and K$_2$CO$_3$ (556 mg, 4.02 mmol) in NMP (10 mL) were placed in a sealed reaction vials and stirred in the microwave reactor at 170 °C for 1 h under an argon atmosphere. The reaction mixture was cooled to room temperature and diluted with CH$_2$Cl$_2$. The organic layer was washed with water, and the aqueous layer was extracted three times with CH$_2$Cl$_2$. The organic layer was combined, dried over Na$_2$SO$_4$, and evaporated under a reduced pressure. The crude product was purified by column chromatography on silica gel (CH$_2$Cl$_2$/EtOAc, 10:1) to give **2** (269 mg, 0.950 mmol) in a 48% yield as brown solids and regioisomer **3** (66.6 mg, 10.2 mmol) as a by-product. Data for **2**: ^{1}H NMR (500 MHz, CDCl$_3$): δ 8.89 (d, *J* = 2.5 Hz, 1H), 8.29 (d, *J* = 3.5 Hz, 1H), 8.17 (d, *J* = 4.0 Hz, 1H), 8.15 (d, *J* = 3.5 Hz, 1H), 7.98 (d, *J* = 2.3 Hz, 1H), 7.83 (d, *J* = 4.0 Hz, 1H), 7.69 (d, *J* = 4.0 Hz, 1H), 7.53 (m, 2H), 7.13 (d, *J* = 4.3 Hz, 1H), and 4.13 (s, 3H); ^{13}C NMR (126 MHz, CDCl$_3$): δ 154.87, 149.92, 139.37, 134.55, 130.59, 130.56, 128.63, 128.20, 127.26, 126.98, 126.38, 124.96, 123.49, 122.03, 120.37, 119.93, 114.06, 108.34, and 56.08 (two sp^2 carbon signals were overlapped with other signals); HRMS (–APCI): [M]$^-$ calculated for C$_{20}$H$_{13}$NO 283.1003, found 283.1007, and found 283.1013. Data for **3**: ^{1}H NMR (500 MHz, CDCl$_3$): δ 8.95 (m, 2H), 8.26 (d, *J* = 3.3 Hz, 1H), 8.04 (d, *J* = 3.5 Hz, 1H), 7.89 (d, *J* = 4.0 Hz, 1H), 7.83 (d, *J* = 4.0 Hz, 1H), 7.67 (m, 3H), 7.56 (dd, *J* = 4.5, 2.5 Hz, 1H), and 4.16 (s, 3H); ^{13}C NMR (126 MHz, CDCl$_3$): δ 155.52, 148.25, 140.07, 138.30, 137.16, 136.77, 132.12, 131.91, 129.42, 128.12, 127.83, 127.72, 126.26, 126.12, 122.46, 122.11, 121.05, 101.91, and 56.21 (one sp^2 signal was overlapped with another signal); HRMS (–APCI): [M]$^-$ calculated for C$_{20}$H$_{13}$NO 283.1003, found 283.1007.

3.3. Synthesis of Compound 4

Compound **1A** (85.3 mg, 0.299 mmol), compound **4A** (196 mg, 0.448 mmol), Pd$_2$(dba)$_3$·CHCl$_3$ (10.0 mg, 0.00966 mmol), PCy$_3$·HBF$_4$ (13.0 mg, 0.0353 mmol) and K$_3$PO$_4$ (191 mg, 0.90 mmol) were suspended in a mixed solvent of DMF/H$_2$O (10:1, 5.5 mL) and stirred for 2 h at 80 °C under an argon atmosphere. The reaction mixture was cooled to room temperature and diluted with CH$_2$Cl$_2$. The organic layer was washed three times with water, and the aqueous layer was extracted three times with CH$_2$Cl$_2$. The organic layer was combined, dried over Na$_2$SO$_4$, and evaporated under a reduced pressure. The crude product was purified by column chromatography on silica gel (CH$_2$Cl$_2$/EtOAc, 10:1) to give **4** (149 mg, 0.290 mmol) in a 97% yield as colorless solids. Data for **4**: ^{1}H NMR (500 MHz, CDCl$_3$): δ 9.00 (dd, *J* = 4.0, 1.5 Hz, 1H), 8.77 (d, *J* = 7.5 Hz, 1H), 8.69 (dd, *J* = 7.0, 1.5 Hz, 1H), 7.87 (dd, *J* = 8.5, 1.0 Hz, 1H), 7.81 (d, *J* = 7.5 Hz, 1H), 7.74 (dd, *J* = 8.5, 1.5 Hz, 1H), 7.64 (t, *J* = 7.8 Hz, 1H), 7.55 (d, *J* = 8.0 Hz, 1H), 7.50 (t, *J* = 7.8 Hz, 1H), 7.35 (m, 3H), 7.24 (d, *J* = 7.5 Hz, 1H), 4.22 (s, 3H), 2.81 (m, 2H), and 1.20 (m, 12H); ^{13}C NMR (126 MHz, CDCl$_3$): δ 187.95, 187.81, 179.74, 172.85, 169.68, 168.24, 163.71, 157.39, 156.68, 155.38, 155.20, 154.94, 154.64, 153.12, 152.96, 152.73, 152.26, 152.07, 151.57, 150.64, 130.82, 79.70, 52.70, 47.30, and 47.25; HRMS (–APCI): [M]$^-$ calculated for C$_{34}$H$_{30}$N$_2$O$_3$ 514.2256, found 514.2244.

3.4. Synthesis of Compound 5

Compound **4** (129 mg, 0.250 mmol) and potassium *tert*-butoxide (168 mg, 1.50 mmol) were suspended in DBU (0.8 mL) and stirred for 1 h at 80 °C under an argon atmosphere. The reaction mixture was cooled to room temperature and quenched with NH$_4$Cl aq. The aqueous layer was extracted three times with CH$_2$Cl$_2$. The organic layer was washed with water, dried over Na$_2$SO$_4$, and evaporated under a reduced pressure. The crude product was purified by column chromatography on silica gel (CH$_2$Cl$_2$/acetone, 10:1) to give **5** (106 mg, 0.208 mmol) in an 83% yield as reddish purple

solids. Data for **5**: ^{1}H NMR (500 MHz, CDCl$_3$): δ 9.01 (d, *J* = 4.5 Hz, 1H), 8.66 (d, *J* = 8.0 Hz, 1H), 8.63 (d, *J* = 8.0 Hz, 1H), 8.57 (d, *J* = 8.0 Hz, 1H), 8.46 (d, *J* = 8.5 Hz, 1H), 8.41 (d, *J* = 8.5 Hz, 1H), 8.24 (d, *J* = 4.5 Hz, 1H), 7.51 (t, *J* = 7.8 Hz, 1H), 7.35 (d, *J* = 7.5 Hz, 1H), 7.24 (d, *J* = 8.5 Hz, 1H), 7.24 (d, *J* = 7.5 Hz, 1H), 4.16 (s, 3H), 2.75 (m, 2H), and 1.14 (d, *J* = 7.0 Hz, 12H); ^{13}C NMR (126 MHz, CD$_2$Cl$_2$): δ 164.30, 158.13, 150.35, 146.50, 141.69, 137.38, 136.96, 135.36, 132.64, 131.84, 131.80, 130.79, 129.73, 127.04, 125.40, 124.59, 124.40, 123.57, 122.15, 121.68, 120.51, 120.22, 116.88, 109.45, 56.74, 30.06, 29.46, and 24.07 (three sp^2 and three sp^3 carbon signals were overlapped with other signals). HRMS (–APCI): [M]$^-$ calculated for C$_{34}$H$_{28}$N$_2$O$_3$ 512.2105, found 512.2095.

3.5. Synthesis of Compound *L1*

MeSNa (106 mg, 1.51 mmol) was weighed in a glove box and placed in a Schlenk tube. Compound **2** (79.8 mg, 0.281 mmol) and DMF (6.0 mL) were added and stirred for 2.5 h at 70 °C under an argon atmosphere. The reaction mixture was cooled to room temperature, diluted with CH$_2$Cl$_2$, and quenched by NH$_4$Cl aq. The organic layer was washed three times with water, and the aqueous layer was extracted three times with CH$_2$Cl$_2$. The organic layer was combined, dried over Na$_2$SO$_4$, and evaporated under a reduced pressure. The aqueous layer was extracted three times with CH$_2$Cl$_2$ again. The crude mixture was dissolved in minimum CH$_2$Cl$_2$, added to *n*-hexane, and filtered with membrane filter to give **L1** (66.1 mg, 0.245 mmol) in an 87% yield as red solids. Data for **L1**: ^{1}H NMR (500 MHz, CDCl$_3$): δ 8.72 (d, *J* = 2.3 Hz, 1H), 8.28 (d, *J* = 3.5 Hz, 1H), 8.15 (m, 2H), 7.96 (d, *J* = 2.5 Hz, 1H), 7.84 (d, *J* = 4.0 Hz, 1H), 7.68 (d, *J* = 4.0 Hz, 1H), 7.53 (m, 2H), and 7.24 (d, *J* = 4.0 Hz, 1H); ^{13}C NMR spectrum could not be obtained due to insufficient solubility; HRMS (–APCI): [M – H]$^-$ calculated for C$_{19}$H$_{10}$NO 268.0768, found 268.0765.

3.6. Synthesis of Compound *L2*

Compound **3** (143 mg, 0.503 mmol) and sodium thiomethoxide (245 mg, 3.50 mmol) were suspended in DMF (5 mL) and stirred for 2 h at 80 °C under an argon atmosphere. The reaction mixture was cooled to room temperature and quenched with NH$_4$Cl aq. The precipitate was filtered and washed with water and MeOH. The crude mixture was dissolved in a minimum amount of CH$_2$Cl$_2$, precipitated with *n*-hexane, and filtered with a membrane filter to give **L2** (127 mg, 0.471 mmol) in a 94% yield as yellow solids. Data for **3**: ^{1}H NMR (500 MHz, CDCl$_3$): δ 8.94 (dd, *J* = 8.0, 1.0 Hz, 1H), 8.77 (dd, *J* = 4.5, 2.0 Hz, 1H), 8.22 (d, *J* = 7.0 Hz, 1H), 8.02 (d, *J* = 7.0 Hz, 1H), 7.88 (d, *J* = 8.0 Hz, 1H), 7.81 (d, *J* = 8.5 Hz, 1H), 7.77 (s, 1H), 7.65 (t, *J* = 7.5 Hz, 2H), and 7.56 (dd, *J* = 8.5, 4.0 Hz, 1H); ^{13}C NMR (126 MHz, CDCl$_3$): δ 152.47, 146.85, 139.52, 138.20, 137.44, 136.89, 132.71, 131.99, 129.53, 128.17, 127.95, 127.94, 126.04, 125.52, 125.02, 122.55, 122.05, 121.51, and 104.46; HRMS (–APCI): [M – H]$^-$ calculated for C$_{19}$H$_{10}$NO 268.0768, found 268.0763.

3.7. Synthesis of Compound *L3*

Compound **5** (590 mg, 1.15 mmol) and sodium thiomethoxide (646 mg, 9.21 mmol) were suspended in DMF (23 mL) and stirred for 2 h at 100 °C under an argon atmosphere. The reaction mixture was cooled to room temperature and quenched with NH$_4$Cl aq. The aqueous layer was extracted three times with CH$_2$Cl$_2$. The organic layer was washed with water, dried over Na$_2$SO$_4$, and evaporated under a reduced pressure. The crude mixture was dissolved in a minimum amount of CH$_2$Cl$_2$, precipitated with *n*-hexane, and filtered with membrane filter to give **L3** (534 mg, 1.07 mmol) in a 93% yield as reddish purple solids. Data for **L3**: ^{1}H NMR (500 MHz, CDCl$_3$): δ 8.91 (d, *J* = 5.0 Hz, 1H), 8.70 (d, *J* = 8.5 Hz, 1H), 8.66 (d, *J* = 8.0 Hz, 1H), 8.53 (d, *J* = 8.0 Hz, 1H), 8.41 (d, *J* = 8.0 Hz, 1H), 8.36 (d, *J* = 8.0 Hz, 1H), 8.22 (d, *J* = 4.5 Hz, 1H), 7.49 (t, *J* = 8.0 Hz, 1H), 7.34 (d, *J* = 8.0 Hz, 2H), 7.33 (d, *J* = 8.5 Hz, 1H), 2.75 (m, 2H), and 1.18 (d, *J* = 6.5 Hz, 12H); ^{13}C NMR (126 MHz, CDCl$_3$): δ 163.86, 163.82, 154.61, 148.97, 145.77, 139.21, 137.63, 137.04, 134.37, 132.67, 131.58, 130.92, 130.56, 129.63, 126.95, 125.61, 124.14, 123.73, 123.59, 121.92, 120.58, 120.21, 119.81, 116.58, 111.86, 29.25, and 24.08 (two sp^2 and four sp^3 carbon

signals were overlapped with other signals); HRMS (–APCI): $[M - H]^-$ calculated for $C_{33}H_{25}N_2O_3$ 497.1865, found 497.1864.

3.8. Synthesis of Compound Al(**L1**)$_3$

Compound **L1** (26.9 mg, 0.0999 mmol) and $AlCl_3$ (5.41 mg, 0.0406 mmol) were suspended in EtOH (1 mL) and stirred for 1 h at reflux temperature under an argon atmosphere. The reaction mixture was quenched with NEt_3. The precipitate was filtered, centrifuged, washed with MeOH, and then it was collected by centrifugation. The resulting solid was dried in vacuo to give **Al(L1)₃** (26.6 mg, 0.0320 mmol) in a 97% yield as dark purple solids. Data for Al(**L1**)$_3$: ^{1}H NMR (500 MHz, 1,1,2,2-tetrachloroethane-d_2): δ 8.70 (m, 2H), 8.22 (m, 4H), 8.15 (d, J = 3.0 Hz, 1H), 8.08 (m, 4H), 7.93 (d, J = 2.3 Hz, 1H), 7.84 (m, 4H), 7.69 (d, J = 2.5 Hz, 1H), 7.61 (m, 3H), 7.49 (m, 6H), 7.39 (d, J = 2.8 Hz, 1H), 7.17 (m, 2H), and 7.10 (d, J = 3.7 Hz, 1H); HRMS (+ESI): $[M + Na]^+$ calculated for $C_{57}H_{30}AlN_3NaO_3$ 854.1995, found 854.1973 (We could not observe the ^{13}C NMR signals of Al(**L1**)$_3$, likely due to severe broadening caused by the aggregation and ligand exchange dynamics.).

3.9. Synthesis of Compound Al(**L3**)$_3$

Compound **L3** (25.0 mg, 0.0501 mmol) and $AlCl_3$ (2.82 mg, 0.0211 mmol) were suspended in EtOH (1 mL) and stirred for 1 h at reflux temperature under an argon atmosphere. The reaction mixture was quenched with NEt_3 and evaporated. The precipitate was centrifuged, washed with MeOH, and then collected by centrifugation. The resulting solid was dried in vacuo to give Al(**L3**)$_3$ (23.2 mg, 0.0153 mmol) in a 92% yield as dark blue solids. Data for Al(**L3**)$_3$: ^{1}H NMR (500 MHz, $CDCl_3$): δ 9.00 (d, J = 5.0 Hz, 1H), 8.93 (d, J = 5.0 Hz, 1H), 8.65 (m, 7H), 8.50 (m, 5H), 8.31 (m, 5H), 8.24 (d, J = 4.5 Hz, 1H), 8.05 (d, J = 4.5 Hz, 1H), 7.62 (d, J = 5.5 Hz, 1H), 7.47 (m, 4H), 7.33 (m, 7H), 2.71 (m, 6H), and 1.16 (m, 36H); HRMS (–APCI): $[M]^-$ calculated for $C_{99}H_{75}AlN_6O_9$ 1518.5416, found 1518.5400 (We could not clearly observe the ^{13}C NMR signals of Al(**L3**)$_3$ likely due to severe broadening caused by the aggregation and ligand exchange dynamics).

4. Conclusions

We have reported a synthetic route to π-extended propeller-shaped tris(8-hydroxyquinoline) aluminum(III) complexes (Alq$_3$), i.e., Al(**L1**)$_3$ and Al(**L3**)$_3$, which contain an azaperylene core in the ligands. A single-crystal X-ray diffraction analysis of Al(**L1**)$_3$ revealed a unique three-dimensional (3D) packing structure, i.e., a two-dimensional honeycomb packing in the *ab*-plane and a one-dimensional π-stacked column along the *c*-axis. In the cyclization of precursor **1** via an intramolecular Pd-catalyzed direct arylation, cyclization modes for the formation of hexagonal and pentagonal rings could be controlled by the use of a catalytic amount of PivOH under a decreased reaction temperature. Al(**L3**)$_3$, which contains strongly electron-withdrawing dicarboximide moieties, was synthesized using a base-promoted cyclization. Al(**L3**)$_3$ exhibited deep blue color in solution with a strong absorption band that extended to 780 nm. Further studies on large propeller-shaped π-systems using metal-coordination for applications in n-type semiconducting materials are currently in progress in our laboratory and will be reported in due course.

Author Contributions: M.T., Y.H., and N.T. performed the experiments and measurements. M.M. (Michihisa Murata), Y.H., and T.S. carried out the X-ray crystallographic analysis. M.M. (Michihisa Murata) and Y.M. designed the experiments. M.T. and M.M. (Michihisa Murata) co-wrote the paper. Y.H., M.M. (Masahiro Muraoka), M.M. (Michihisa Murata), T.S., A.W., and Y.M. reviewed and approved the final manuscript. All authors contributed to the discussions.

References

1. Zhang, Z.; Burkholder, E.; Zubieta, J. Non-merohedrally twinned crystals of *N,N′*-bis(3-methylphenyl)-*N,N′*-diphenyl-1,1′-biphenyl-4,4′-diamine: An excellent triphenylamine-based hole transporter. *Acta Crystallogr. Sect. C Cryst. Struct. Commun.* **2004**, *60*, 452–454. [CrossRef] [PubMed]

2. Wakamiya, A.; Nishimura, H.; Fukushima, T.; Suzuki, F.; Saeki, A.; Seki, S.; Osaka, I.; Sasamori, T.; Murata, M.; Murata, Y.; et al. On-Top π-Stacking of Quasiplanar Molecules in Hole-Transporting Materials: Inducing Anisotropic Carrier Mobility in Amorphous Films. *Angew. Chem.* **2014**, *126*, 5910–5914. [CrossRef]

3. Nishimura, H.; Ishida, N.; Shimazaki, A.; Wakamiya, A.; Saeki, A.; Scott, L.T.; Murata, Y. Hole-Transporting Materials with a Two-Dimensionally Expanded π-System around an Azulene Core for Efficient Perovskite Solar Cells. *J. Am. Chem. Soc.* **2015**, *137*, 15656–15659. [CrossRef] [PubMed]

4. Zhong, Y.; Kumar, B.; Oh, S.; Trinh, M.T.; Wu, Y.; Elbert, K.; Li, P.; Zhu, X.; Xiao, S.; Ng, F.; et al. Helical Ribbons for Molecular Electronics. *J. Am. Chem. Soc.* **2014**, *136*, 8122–8130. [CrossRef] [PubMed]

5. Lv, L.; Roberts, J.; Xiao, C.; Jia, Z.; Jiang, W.; Zhang, G.; Risko, C.; Zhang, L. Triperyleno[3,3,3]propellane triimides: Achieving a new generation of quasi-D3h symmetric nanostructures in organic electronics. *Chem. Sci.* **2019**, *10*, 4951–4958. [CrossRef] [PubMed]

6. Li, H.; Earmme, T.; Ren, G.; Saeki, A.; Yoshikawa, S.; Murari, N.M.; Subramaniyan, S.; Crane, M.J.; Seki, S.; Jenekhe, S.A. Beyond Fullerenes: Design of Nonfullerene Acceptors for Efficient Organic Photovoltaics. *J. Am. Chem. Soc.* **2014**, *136*, 14589–14597. [CrossRef] [PubMed]

7. Menke, E.H.; Lami, V.; Vaynzof, Y.; Mastalerz, M. π-Extended rigid triptycene-trisaroylenimidazoles as electron acceptors. *Chem. Commun.* **2016**, *52*, 1048–1051. [CrossRef] [PubMed]

8. Meng, D.; Fu, H.; Fan, B.; Zhang, J.; Li, Y.; Sun, Y.; Wang, Z. Rigid Nonfullerene Acceptors Based on Triptycene-Perylene Dye for Organic Solar Cells. *Chem. Asian J.* **2017**, *12*, 1286–1290. [CrossRef] [PubMed]

9. Schneider, A.M.; Wu, Q.; Zhao, D.; Chen, W.; Yu, L. Covalently Bound Clusters of Alpha-Substituted PDI—Rival Electron Acceptors to Fullerene for Organic Solar Cells. *J. Am. Chem. Soc.* **2016**, *138*, 7248–7251.

10. Gao, G.; Liang, N.; Geng, H.; Jiang, W.; Fu, H.; Feng, J.; Hou, J.; Feng, X.; Wang, Z. Spiro-Fused Perylene Diimide Arrays. *J. Am. Chem. Soc.* **2017**, *139*, 15914–15920. [CrossRef]

11. Zhang, J.; Li, Y.; Huang, J.; Hu, H.; Zhang, G.; Ma, T.; Chow, P.C.Y.; Ade, H.; Pan, D.; Yan, H. Ring-Fusion of Perylene Diimide Acceptor Enabling Efficient Nonfullerene Organic Solar Cells with a Small Voltage Loss. *J. Am. Chem. Soc.* **2017**, *139*, 16092–16095. [CrossRef] [PubMed]

12. Peurifoy, S.R.; Castro, E.; Liu, F.; Zhu, X.-Y.; Ng, F.; Jockusch, S.; Steigerwald, M.L.; Echegoyen, L.; Nuckolls, C.; Sisto, T.J. Three-Dimensional Graphene Nanostructures. *J. Am. Chem. Soc.* **2018**, *140*, 9341–9345. [CrossRef] [PubMed]

13. Tang, C.W.; Vanslyke, S.A. Organic Electroluminescent Diodes. *Appl. Phys. Lett.* **1987**, *51*, 913–915. [CrossRef]

14. Desai, P.; Shakya, P.; Kreouzis, T.; Gillin, W.; Morley, N.; Gillin, W.P.; Morley, N.A.; Gibbs, M.R.J. Magnetoresistance and efficiency measurements of Alq3-based OLEDs. *Phys. Rev. B* **2007**, *75*, 094423. [CrossRef]

15. Utz, M.; Nandagopal, M.; Mathai, M.; Papadimitrakopoulos, F. Characterization of isomers in aluminum tris(quinoline-8-olate) by one-dimensional [sup 27]Al nuclear magnetic resonance under magic-angle spinning. *Appl. Phys. Lett.* **2003**, *83*, 4023. [CrossRef]

16. Utz, M.; Chen, C.; Morton, M.; Papadimitrakopoulos, F. Ligand Exchange Dynamics in Aluminum Tris-(Quinoline-8-olate): A Solution State NMR Study. *J. Am. Chem. Soc.* **2003**, *125*, 1371–1375. [CrossRef] [PubMed]

17. Kaji, H.; Kusaka, Y.; Onoyama, G.; Horii, F. CP/MAS13C NMR Characterization of the Isomeric States and Intermolecular Packing in Tris(8-hydroxyquinoline) Aluminum(III) (Alq3). *J. Am. Chem. Soc.* **2006**, *128*, 4292–4297. [CrossRef] [PubMed]

18.	Pohl, R.; Anzenbacher, P. Emission Color Tuning in AlQ₃ Complexes with Extended Conjugated Chromophores. *Org. Lett.* **2003**, *5*, 2769–2772. [CrossRef] [PubMed]

19.	Qin, Y.; Kiburu, I.; Shah, S.; Jäkle, F. Luminescence Tuning of Organoboron Quinolates through Substituent Variation at the 5-Position of the Quinolato Moiety. *Org. Lett.* **2006**, *8*, 5227–5230. [CrossRef]

20.	D'Souza, F.; Maligaspe, E.; Zandler, M.E.; Subbaiyan, N.K.; Ohkubo, K.; Fukuzumi, S. Metal Quinolinolate-Fullerene(s) Donor-Acceptor Complexes: Evidence for Organic LED Molecules Acting as Electron Donors in Photoinduced Electron-Transfer Reactions. *J. Am. Chem. Soc.* **2008**, *130*, 16959–16967. [CrossRef]

21.	Zlojutro, V.; Hudson, Z.M.; Sun, Y.; Wang, S. Triarylboron-functionalized 8-hydroxyquinolines and their aluminium(iii) complexes. *Chem. Commun.* **2011**, *47*, 3837. [CrossRef] [PubMed]

22.	Chen, Y.; Wang, H.; Wan, L.; Bian, Y.; Jiang, J. 8-Hydroxyquinoline-Substituted Boron–Dipyrromethene Compounds: Synthesis, Structure, and OFF–ON–OFF Type of pH-Sensing Properties. *J. Org. Chem.* **2011**, *76*, 3774–3781. [CrossRef] [PubMed]

23.	Zhao, X.; Wang, S.; Zhang, L.; Liu, S.; Yuan, G. 8-Hydroxyquinolinate-Based Metal–Organic Frameworks: Synthesis, Tunable Luminescent Properties, and Highly Sensitive Detection of Small Molecules and Metal Ions. *Inorg. Chem.* **2019**, *58*, 2444–2453. [CrossRef] [PubMed]

24.	Campeau, L.-C.; Parisien, M.; Jean, A.; Fagnou, K. Catalytic Direct Arylation with Aryl Chlorides, Bromides, and Iodides: Intramolecular Studies Leading to New Intermolecular Reactions. *J. Am. Chem. Soc.* **2006**, *128*, 581–590. [CrossRef] [PubMed]

25.	Lafrance, M.; Fagnou, K. Palladium-Catalyzed Benzene Arylation: Incorporation of Catalytic Pivalic Acid as a Proton Shuttle and a Key Element in Catalyst Design. *J. Am. Chem. Soc.* **2006**, *128*, 16496–16497. [CrossRef] [PubMed]

26.	Gorelsky, S.I.; Lapointe, D.; Fagnou, K. Analysis of the Concerted Metalation-Deprotonation Mechanism in Palladium-Catalyzed Direct Arylation across a Broad Range of Aromatic Substrates. *J. Am. Chem. Soc.* **2008**, *130*, 10848–10849. [CrossRef]

27.	Baghbanzadeh, M.; Pilger, C.; Kappe, C.O. Palladium-Catalyzed Direct Arylation of Heteroaromatic Compounds: Improved Conditions Utilizing Controlled Microwave Heating. *J. Org. Chem.* **2011**, *76*, 8138–8142. [CrossRef] [PubMed]

28.	Alberico, D.; Scott, M.E.; Lautens, M. Aryl–Aryl Bond Formation by Transition-Metal-Catalyzed Direct Arylation. *Chem. Rev.* **2007**, *107*, 174–238. [CrossRef]

29.	Neufeldt, S.R.; Sanford, M.S. Controlling Site Selectivity in Palladium-Catalyzed C–H Bond Functionalization. *Acc. Chem. Res.* **2012**, *45*, 936–946. [CrossRef]

30.	Tan, Y.; Hartwig, J.F. Assessment of the Intermediacy of Arylpalladium Carboxylate Complexes in the Direct Arylation of Benzene: Evidence for C–H Bond Cleavage by "Ligandless" Species. *J. Am. Chem. Soc.* **2011**, *133*, 3308–3311. [CrossRef]

31.	Seifert, S.; Schmidt, D.; Shoyama, K.; Würthner, F. Base-Selective Five- versus Six-Membered Ring Annulation in Palladium-Catalyzed C–C Coupling Cascade Reactions: New Access to Electron-Poor Polycyclic Aromatic Dicarboximides. *Angew. Chem. Int. Ed.* **2017**, *56*, 7595–7600. [CrossRef] [PubMed]

32.	Frisch, M.J.; Trucks, G.W.; Schlegel, H.B.; Scuseria, G.E.; Robb, M.A.; Cheeseman, J.R.; Scalmani, G.; Barone, V.; Mennucci, B.; Petersson, G.A.; et al. *Gaussian 09, Revision E.01*; Gaussian, Inc.: Wallingford, CT, USA, 2013.

33.	Ueda, K.; Yanagisawa, S.; Yamaguchi, J.; Itami, K. A General Catalyst for the β-Selective C–H Bond Arylation of Thiophenes with Iodoarenes. *Angew. Chem. Int. Ed.* **2010**, *49*, 8946–8949. [CrossRef] [PubMed]

34.	Tang, S.-Y.; Guo, Q.-X.; Fu, Y. Mechanistic Origin of Ligand-Controlled Regioselectivity in Pd-Catalyzed C-H Activation/Arylation of Thiophenes. *Chem. A Eur. J.* **2011**, *17*, 13866–13876. [CrossRef] [PubMed]

35.	Hashikawa, Y.; Murata, M.; Wakamiya, A.; Murata, Y. Palladium-Catalyzed Cyclization: Regioselectivity and Structure of Arene-Fused C60 Derivatives. *J. Am. Chem. Soc.* **2017**, *139*, 16350–16358. [CrossRef] [PubMed]

36.	Ohkawara, T.; Suzuki, K.; Nakano, K.; Mori, S.; Nozaki, K. Facile Estimation of Catalytic Activity and Selectivities in Copolymerization of Propylene Oxide with Carbon Dioxide Mediated by Metal Complexes with Planar Tetradentate Ligand. *J. Am. Chem. Soc.* **2014**, *136*, 10728–10735. [CrossRef] [PubMed]

37.	Andrew, T.L.; VanVeller, B.; Swager, T.M. The Synthesis of Azaperylene-9,10-dicarboximides. *Synlett* **2010**, *2010*, 3045–3048.

38.	Sakamoto, T.; Pac, C. A "Green" Route to Perylene Dyes: Direct Coupling Reactions of 1,8-Naphthalimide and Related Compounds under Mild Conditions Using a "New" Base Complex Reagent, *t*-BuOK/DBN. *J. Org. Chem.* **2001**, *66*, 94–98. [CrossRef] [PubMed]
39.	Amati, M.; Lelj, F. Monomolecular isomerization processes of aluminum tris(8-hydroxyquinolinate) (Alq3): A DFT study of gas-phase reaction paths. *Chem. Phys. Lett.* **2002**, *363*, 451–457. [CrossRef]
40.	Katakura, R.; Koide, Y. Configuration-Specific Synthesis of the Facial and Meridional Isomers of Tris(8-hydroxyquinolinate)aluminum (Alq3). *Inorg. Chem.* **2006**, *45*, 5730–5732. [CrossRef]
41.	Brinkmann, M.; Gadret, G.; Muccini, M.; Taliani, C.; Masciocchi, N.; Sironi, A. Correlation between Molecular Packing and Optical Properties in Different Crystalline Polymorphs and Amorphous Thin Films of mer-Tris(8-hydroxyquinoline)aluminum(III). *J. Am. Chem. Soc.* **2000**, *122*, 5147–5157. [CrossRef]
42.	Hummelen, J.C.; Knight, B.W.; LePeq, F.; Wudl, F.; Yao, J.; Wilkins, C.L. Preparation and Characterization of Fulleroid and Methanofullerene Derivatives. *J. Org. Chem.* **1995**, *60*, 532–538. [CrossRef]
43.	Morinaka, Y.; Nobori, M.; Murata, M.; Wakamiya, A.; Sagawa, T.; Yoshikawa, S.; Murata, Y. ChemInform Abstract: Synthesis and Photovoltaic Properties of Acceptor Materials Based on the Dimerization of Fullerene C 60 for Use in Efficient Polymer Solar Cells. *Chem. Commun.* **2013**, *49*, 3670–3672. [CrossRef] [PubMed]